Analysis of the Detuning Regulation of a Double-Pumped Microcavity

X. Xu, H. C. Ye, X. Y. Jin, D. Chen, and H. J. Xia

***Abstract*—The detuning regulation of a double-pumped microcavity is investigated. In this paper, results show that one of the detuning parameters' regulation facilitates dual-comb generation. When the other detuning parameter is selected appropriately, dual fields of solitons and Turing patterns generate simultaneously during the detuning. In this case, dual combs with a relatively large repeat frequency difference appear by use of a microcavity. Moreover, properly fast detuning is propitious for stable field evolutions, whereas slow detuning can lead to solitons and Turing patterns drift. Moreover, after the generation of solitons and Turing patterns in the detuning, the method of suddenly stabilizing the detuning parameter to a certain value is used to sustain or regulate the existing fields. When the fixed value of mutation is small, the coexistence of solitons and Turing patterns can be maintained all the time and the large variation value of the detuning parameter results in dual solitons in the microcavity. The results of this paper provide a new approach to excite dual combs taking advantage of a single microcavity.**

***Index Terms*—Double-pumped microcavity, dual combs, frequency combs, Lugiato-Lefever equation.**

I. Introduction

MICROCAVITY-BASED optical frequency combs have attracted extensive interests due to their compactness, flexibility, low power consumption, and compatibility with CMOS integration [1], [2], [3], [4]. Compared with conventional frequency combs based on mode-locked laser, microcavity-based frequency combs not only create an ultra-wide broadband spectrum but also extend the frequency interval between modes to the order of GHz [5], [6], [7], [8]. Furthermore, a variety of materials [9], [10], [11], [12] provide a promising platform for extensive applications [13], [14], [15], [16], for example, optical communications and interconnects, optical phased array-based LiDAR, sensors for chemical and biological analysis, integrated quantum technologies, and finally, optical computing [17]. In recent years, with the continuous development of microcavity-based frequency combs, the dual-comb system has become a new research topic. For optical ranging, a dual-comb distance measurement enables the in-flight sampling of dynamic projectiles moving at 150 m/s [18]. In the field of spectroscopy research, dual-comb spectroscopy has emerged as a powerful approach to acquire nearly instantaneous Raman and optical spectra with unprecedented resolution [19]. In addition, the dual-comb system based on microcavities has been applied to image static and moving targets [20]. Moreover, the synergy of broad spectral bandwidth and high temporal coherence provided by the dual-comb system opens up novel hyperspectral digital holography [21].

At present, investigation has been performed to generate dual combs. For some particular applications, dual optical frequency combs with several times the difference in repetition frequency are required. The widely used approach is to integrate two microcavities into one optical system, which is pumped by two separate laser sources [22], [23], [24]. For example, in the microfabricated photonic optical atomic clock, it consists of interlocked dissipative soliton combs generated using silica microresonator of 2 mm diameter, and a 46 μm diameter, Si_3N_4 microresonator [25]. This pair of interlocked Kerr frequency combs provide fully coherent optical division of the clock laser to generate an electronic 22 GHz clock signal with a fractional frequency instability of one part in 10^{13}. Although this system can be exploited to produce dual combs with slight repeat frequency difference, precise fabrication processes are required to control strictly the free spectral range (FSR), which is dependent on the geometry of the microcavities. Moreover, the current polishing or laser processes in the microcavity processing cannot guarantee the accuracy of the fabrication [26]. In addition, the frequency locking system of the dual microcavities would be more complex. The method of generating two combs from a single microcavity is employed. By combining Kerr and Brillouin nonlinearities in an over-modal microcavity, the dual-comb modes are selected, the repetition rate difference of a dual-comb pair could be flexibly switched, ranging from 8.5 to 212 MHz [27]. Furthermore, via exciting the intracavity Brillouin laser in a high Q monolithic fiber resonator, a pair of orthogonal Kerr soliton combs is generated, which share the same repetition due to the soliton trapping but different central wavelengths [28]. For simplicity, in such experimental setup, only one pump is used, and its frequency shifts by the use of an electro- or acousto-optic modulator [29]. Thus, in a microcavity, clockwise and counter-clockwise modes, which are in the same

Manuscript received 26 September 2023; revised 3 November 2023; accepted 20 November 2023. Date of publication 28 November 2023; date of current version 11 December 2023. This work was supported in part by the National Natural Science Foundation of China under Grant 52175503. *(Corresponding author: X. Y. Jin.)*

X. Xu, X. Y. Jin, D. Chen, and H. J. Xia are with the Anhui Province Key Laboratory of Measuring Theory and Precision Instrument, School of Instrument Science and Optoelectronics Engineering, Hefei University of Technology, Hefei 230009, China (e-mail: xuxin@hfut.edu.cn; xyjin007@hfut.edu.cn; dchen@hfut.edu.cn; hjxia@hfut.edu.cn).

H. C. Ye is with the Department of Precision Machinery and Precision Instrumentation, University of Science and Technology of China, Hefei 230026, China (e-mail: huichun@ustc.edu.cn).

Digital Object Identifier 10.1109/JPHOT.2023.3335963

© 2023 The Authors. This work is licensed under a Creative Commons Attribution-NonCommercial-NoDerivatives 4.0 License. For more information, see https://creativecommons.org/licenses/by-nc-nd/4.0/

operating regime, are excited simultaneously [30], [31]. Taking advantage of the cross-phase modulation (XPM) effect, only a small frequency difference between the dual combs can be achieved [32].

For a single microcavity, coherent dual combs with significant repetition frequency differences can be generated by pumping different spatial modes, which are in the same direction. The resonant frequencies of the two modes, which are determined by the structure and dispersion of the microcavity, are identical. Moreover, another pumping method is proposed. The microcavity is pumped by two independent lasers, whose polarizations are completely orthogonal [33], [34], [35]. This setup allows for the excitation of two modes inside the microcavity. In previous studies, only soliton formation with dual pumps was discussed [36]. The resonant frequencies of the two modes, which are determined by the structure and dispersion of the microcavity, are identical. However, because the parameters of the two pumps can be set individually, the detuning of the two modes is different. Thus, the dual propagating modes can operate in various states. It results in the formation of two combs in the microcavity, whose repetition frequency differences can reach a wider range of several FSRs. Accordingly, with the help of the separate control of the two pumps, a large repetition frequency difference between the dual combs can be achieved.

In this paper, detuning regulation facilitates the excitation of different forms of the field distributions of a double-pumped microcavity. To study the effect of specific detuning parameters, the theoretical model of coupled Lugiato–Lefever Equation (LLE) is introduced. The frequency of one of the pumps is regulated, the other pump frequency is keep constant, the evolutions of the dual fields with orthogonal polarization are demonstrated. Consequently, the dual Turing patterns can appear at the same time, and more meaningfully, the two fields can exhibit solitons and Turing patterns simultaneously. Furthermore, to obtain stable fields, the influence of detuning regulation speed on spatial and temporal evolution is discussed. Properly fast detuning facilitates stable field evolutions, whereas slow detuning can lead to solitons and Turing patterns drift. For the desirable situation of coexistence of solitons and Turing patterns, the original fields can be sustained by abruptly changing the detuning parameters. The result of detuning mutation is small, and the original field of the coexistence of solitons and Turing patterns remains constant. Moreover, the large variation value of the detuning parameter leads to dual solitons. The results of this paper are important for studying the fields in a double-pumped microcavity. It provides a new approach to excite dual combs with a large difference in repetition frequency by use of a single microcavity.

II. Theoretical Model

In conventional optical microcavities with a single pump, the formation of the frequency combs inside the microcavities is typically characterized by the well-known LLE [37], [38]. In this theoretical model of the microcavities, the frequency of the pumping mode is ω_0. Hence, the resonant frequencies of the μ-th mode ω_μ can be described as the following Taylor expansion [39]:

$$\omega_\mu = \omega_0 + D_1\mu + \frac{1}{2}D_2\mu^2 + \ldots + \frac{1}{n!}D_n\mu^n + \ldots \quad (1)$$

where D_1 is the intermodal angular frequency or FSR of the microcavities, and D_2 is the second-order dispersion coefficient.

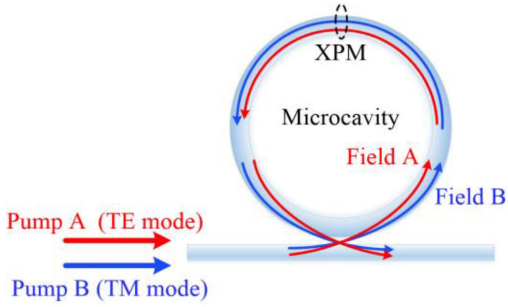

Fig. 1. Illustration of an orthogonally polarized double-pumped microcavity. The two pump modes are TM mode and TE mode, and XPM plays an important role between the dual propagating fields.

In a double-pumped microcavity, the simulation model is exhibited in Fig. 1. For the excitation of dual combs that can be distinguished, dual pumps with orthogonal polarization are employed. They are TE modes and TM modes, which are marked as pumps A and B, respectively. The resulting fields are referred to as fields A and B. The dual propagating fields inside microcavity interact via XPM effects [40].

With the interaction of two fields, dual frequency combs can be established in the microcavities. To describe the evolution of the dual frequency combs, two coupled LLEs are introduced, in which the dual complex fields A and B with orthogonal polarizations are expressed as follows [36]:

$$\frac{\partial A(\phi,\tau)}{\partial \tau} = -(1+i\alpha_A)A + i\beta_A\frac{\partial^2 A}{\partial \phi^2} + i\left(|A|^2 + \sigma|B|^2\right) \times A + \gamma\frac{\partial A}{\partial \phi} + F_A \quad (2)$$

$$\frac{\partial B(\phi,\tau)}{\partial \tau} = -(1+i\alpha_B)B + i\beta_B\frac{\partial^2 B}{\partial \phi^2} + i\left(|B|^2 + \sigma|A|^2\right) \times B - \gamma\frac{\partial B}{\partial \phi} + F_B \quad (3)$$

where ϕ is the azimuth angle of the microcavities, τ is the slow time, α_* is the detuning parameter, $\beta_* = -2D_{2*}/\Delta\omega_{tot}$ relates to the dispersion parameter, $\Delta\omega_{tot}$ is the total line widths, σ represents the XPM coefficient, $\gamma = (D_{1b}-D_{1a})/\kappa$, κ is the microcavity decay, and F_* is the intensity of the dual pump. The symbol $(_*)$ represents A or B. By solving (2) and (3), the evolution of the dual fields A and B in the microcavities can be obtained separately.

III. Dual Frequency Combs With Detuning Regulation

In general, the frequency combs can be excited only when the frequency detuning satisfy certain conditions, which are dependent on the material and structure of the microcavities [38],

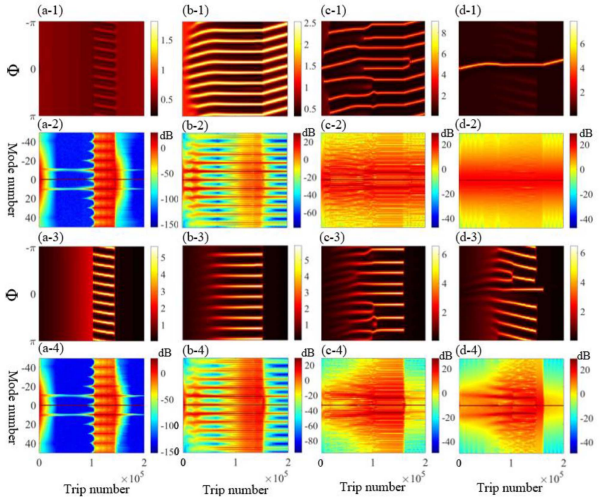

Fig. 2. Temporal and spectral evolutions of the dual combs in the regulation of detuning parameter α_B. The four diagrams in the same vertical row represent in turn the temporal distribution of the first field *A*, the spectrum evolution of the first field *A*, the temporal distribution of the second field *B*, and the spectrum evolution of the second field *B*. (a) $\alpha_A = -1.2$, (b) $\alpha_A = 0.4$, (c) $\alpha_A = 2.2$, and (d) $\alpha_A = 2.6$.

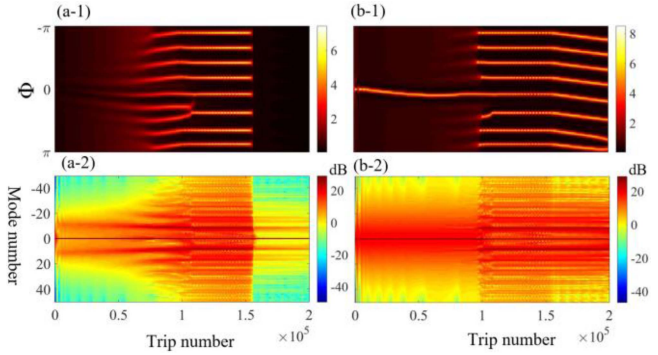

Fig. 3. Evolutions of *A* and *B* fields and spectra with $\alpha_B = 2.4$ and α_A scanning range of −2–5. (a-1) Temporal evolution of field *A*, (a-2) Spectral evolution of field *A*, (b-1) Temporal evolution of field *B*, and (b-2) Spectral evolution of field *B*.

[39]. In practice, for the sake of the frequency comb formation, frequency detuning is usually regulated by means of scanning the pump wavelength [43], [44].

In our simulation, the detuning of the first pump wavelength remains constant during the second pump wavelength scanning. Then, for the detuning parameters, α_A is a fixed value, and α_B scans with time. For the excitation of the field, we chose to artificially inject a soliton pulse. Thus, the initial field in microcavities is supposed to be a weak Gaussian pulse. In addition, the simulation parameters are configured as $\beta_A = \beta_B = -0.05$, $\gamma = 0.01$, $F_A = F_B = 1.5$, and $\sigma = 2/3$ because of dual pump modes with orthogonal polarizations [45]. The detuning parameter α_B is scanned in the range of −2 to 5; α_A is taken as −1.2, 0.4, 2.2, and 2.6.

The spatial and temporal evolution of the dual combs are demonstrated in Fig. 2. The magnitude of detuning parameter α_A affects the evolution of the dual fields. In Fig. 2(a-1)–(a-4), due to the strong negative detuning of the first field ($\alpha_A = -1.2$), both fields only briefly experience Turing patterns during the regulation of α_B. The dual fields have a similar form, but the larger detuning of the *A* leads to its greater loss and weaker power than field *B*. The region where the Turing patterns emerge corresponds to α_B in an approximate range of 1.5 to 3.2. In the corresponding spectral region, combs with 10 mode intervals is obtained. When field *A* is in the weaker positive detuning state (Fig. 2(b-1)–(b-4), $\alpha_A = 0.4$), both fields develop stable Turing patterns. However, as α_B detuning increases, field *B* evolves into a weak Turing pattern, which is not evident in the time domain diagram (Fig. 2(b-3)) but can be seen in the spectrogram. In Fig. 2(b-4), the trip number exceeds the range of 1.5×10^5, and the presence of widely spaced combs in the spectrum indicates that Turing patterns still persist at this time. Field *A* still maintains visible Turing patterns, but the pulse position shifts uniformly with time, which is attributed to the relatively large difference in detuning between the dual fields in this time period. In Figs. 2(c-1)–(c-4), α_B further increases, and the field evolutions present some irregular pulses due to the enhanced modulation instability effect of the dual fields. Owing to the larger value of α_A, the greater amount of α_B near the end of the loop leads to a weaker Turing patterns strength in field *A* and an eventual weak DC distribution of field *B*. In Fig. 2(d-1)–(d-4), α_A is equal to 2.6, and a substantial phenomenon is generated. Throughout the regulation of α_B, field *A* consistently maintains a stable single pulse, which is the notable soliton, and a broadband comb spectrum is derived. As a result, the nonlinear effects, frequency detuning, pump gain, intrinsic loss, and coupling effects of the two fields are balanced for field *A*. Field *B* experiences a gradually increasing field, whose distribution is approximate to Turing patterns. The position of the intermediate pulse is kept invariant owing to the coupling effect of field *A*, and the other pulses drift with time because of the combined effect of the two frequency detuning. Similarly, the Turing patterns vanish when the detuning effect of field *B* is excessively strong.

Moreover, the field evolution under the effect of α_A detuning is studied. In field evolution (2) and (3), only the positive and negative signs of one of the terms in the equation differ. Accordingly, the evolutions of the dual fields are similar to the results in Fig. 2, and only a distinctive result is presented in Fig. 3. When α_B is 2.4, the scanning range of α_A is also −2 to 5, and field *A* gradually results in Turing patterns from the weak DC distribution. Nevertheless, field *B* evolves from the initial field to a soliton pulse. Eventually, field *A* is transformed into a DC distribution under the effect of detuning regulation, and field *B* is drifting Turing patterns.

The above investigation discovers that by selecting different values for one of the pumping wavelengths, various field forms can be excited during the scanning of the other pump wavelength. In particular, solitons and Turing patterns can coexist reliably in microcavities, which has important implications for the application of microcavities in practice. In the case of dual pumping, two different comb spectra can be created by use of a single microcavity, which facilitates frequency synthesis as well as various precision measurement applications.

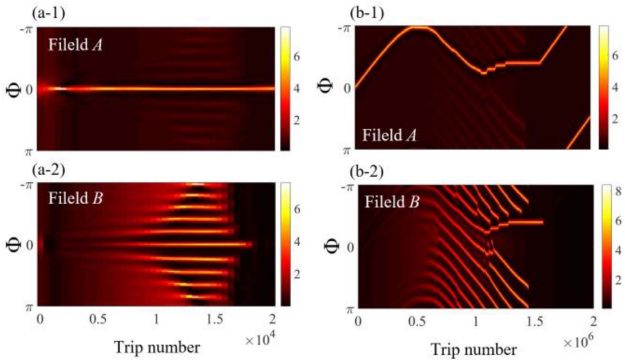

Fig. 4. Evolution of fields A and B at different detuning regulation speeds. (a-1) (a-2) α_B scans at 10x speed, (b-1) (b-2) α_B scans at 0.1x speed. The scanning range is from -2 to 5.

IV. Influence of Detuning Regulating Speed on Spatial and Temporal Evolution

As a result of the remarkable contribution of solitons, this paper focuses on the case of soliton existence. The scanning speed of the pump wavelength still affects the generation of optical frequency combs. Because if the scanning speed is relatively fast, the nonlinearities, dispersion, losses and coupling in the microcavity do not have time to reach equilibrium, and the optical field will become irregular due to excessive detuning. Conversely, when the pump wavelength is scanned slowly, the various effects within the microcavity have time to reach relative stability. In other words, although the final detuning is the same, the strength of the nonlinear, dispersion, coupling and other effects in the intermediate processes are all different. Therefore, the influence of detuning regulating speed on spatial and temporal evolution needs to be studied.

Based on the simulation results in Fig. 2(d-1) and (d-3), in which the solitons in field A are always continuously maintained throughout the detuning regulation, the influence of detuning regulating speed on spatial and temporal evolution is researched. The value of α_A remains 2.6 in Fig. 2(d), and the scanning range of α_B is still -2–5. The values of α_B are selected as 0.1x and 10x scan speed, and the evolutions of fields A and B are illustrated in Fig. 4. The modification of the detuning rate does not affect the form of the field evolution, although distinctions remain. In case of 10x scanning speed, field A can consistently have a stable soliton, which does not undergo spatial drift compared with the soliton in Fig. 2(d-1). Field B suffers from gradually increasing Turing patterns and finally converts to a DC distribution due to detuning overload. When 0.1x scanning speed is selected, a more dramatic drift of the pulse is presented in Fig. 4(b-1) compared with that in Fig. 2(d-1). For field B, the superposition of Turing patterns and solitons evolve from the drifting Turing patterns. Finally, analogous to Fig. 2(d-1), when the solitons in the optical field B vanish, a drifting soliton pulse is generated in field A. According to our findings, to maintain the coexistence of Turing rings and single soliton, the scanning speed of α_B needs to be controlled between 0.89x and 1.26x speed. Consequently, the appropriate fast scanning facilitates the formation of invariant solitons in the microcavities.

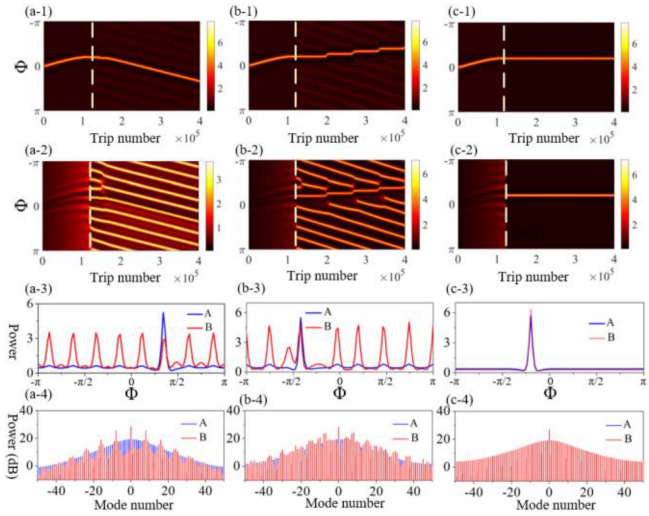

Fig. 5. Regulated results of soliton. The four diagrams in the same vertical row represent the temporal evolution of field A, the temporal evolution of field B, the final field distributions of fields A and B, and the ultimate spectra of fields A and B. The dashed yellow lines indicate the moment when α_B suddenly changes. The values of α_B after the sudden modification are (a) $\alpha_B = 1$, (b) $\alpha_B = 2$, and (c) $\alpha_B = 3$, separately.

V. Sustaining and Regulation of the Soliton

Based on the above analysis, detuning regulation is beneficial for excitation of solitons in microcavities with dual pumps, but after the solitons are activated, sustaining the solitons is a critical issue. When the soliton is developed, the detuning parameter is fixed at a specific value that enables sustaining the stability of the fields in microcavities. The fixed value of detuning is different, and the resulting stable fields are not the exact same. It is also still based on the results of Fig. 2(d-1)–(d-4) to investigate how to maintain the soliton.

In Fig. 2(d-1)–(d-4), during the detuning when the trip number is equal to 1.2×10^5, the state of field A is a soliton, and field B is Turing patterns. At this point, the value of α_B scans to 2.2. Then, the value of α_B is suddenly replaced by a specific amount, which determines the subsequent form of the fields. When α_B mutates to 1, the variation of fields A and B is illustrated in Fig. 5(a-1) and (a-2), where the dashed yellow lines correspond to the moment when α_B suddenly changes. Fig. 5(a-3) and (a-4) are the field distributions and the corresponding spectra at the terminal moment, respectively. After α_B is fixed at 1, field B evolves into more visible Turing patterns, which contain eight identically spaced pulses. Field A is still a drifting soliton, whose shift speed is the same as that of the Turing patterns in field B. In correspondence to the spectrum, optical field A is a broadband comb spectrum. The spectrum of field B has eight mode intervals between two adjacent peaks.

In Fig. 5(b-1)–(b-4), α_B is abruptly changed to 2. As a result of the coupling effect between the two pump modes, field A turns into stepped solitons, which also affect the distribution of Turing patterns in field B. The drifting pulses in field B are interrupted by solitons, which leads to an irregular spectrum. When the value of α_B changes to 3, an interesting consequence is generated, which is shown in Fig. 5(c-1)–(c-4). Dual identical

stable solitons appear, and two sets of broadband combs spectra are in the microcavities. But there's a slight difference in the intensity of the two pulses. The pulse peak in field *A* is slightly higher than in *B*.

The above analysis proves that the detuning parameters abruptly change during the detuning, which is able to regulate the existing fields. In the regulation of available soliton and Turing patterns, the detuning parameter is adjusted to a smaller value, and the original fields remain unchanged. However, the large variation value of the detuning parameter contributes to the generation of two solitons. The changed detuning parameter is close to the original value, and field *B* becomes a superposition of solitons and Turing patterns due to the coupling effect.

VI. Conclusion

In conclusion, a microcavity pumped by dual lasers with orthogonal polarization can generate dual-frequency combs, and detuning regulation is beneficial for the excitation of different forms of dual field distributions. Therefore, based on coupled LLE, the field evolutions in a double-pumped microcavity are investigated theoretically. The wavelength of one of the dual pumps is scanned, that is, the detuning parameter of one field mode is regulated separately. A detuning range from -2 to 5 is selected. By determining different values for the other detuning parameter, various field evolutions can be obtained. Consequently, dual Turing patterns can appear and disappear simultaneously. More notable is that solitons and Turing patterns can coexist reliably in a microcavity, which facilitates frequency synthesis as well as various precision measurement applications.

The influence of detuning regulation speed on spatial and temporal evolution is also discussed. Based on the results of the coexistence of solitons and Turing patterns, the scan of detuning is changed to 10x speed, and more stable field distributions without drift are achieved. Scanning at 0.1x speed, the drift of the fields are more dramatic. Hence, properly fast detuning facilitates a stable field evolution.

To maintain the simultaneous presence of solitons and Turing patterns in the microcavity, the method of suddenly stabilizing the detuning parameter to a certain value is used. During the detuning process, the detuning parameter is abruptly changed to a fixed value after the solitons and Turing patterns generate. The result of detuning mutation is small, the original field of the coexistence of solitons and Turing patterns remains constant, and the large variation value of the detuning parameter leads to dual solitons. These research results promote the remarkable development of a double-pumped microcavity.

References

[1] A. R. Johnson et al., "Chip-based frequency combs with sub-100 GHz repetition rates," *Opt. Lett.*, vol. 3, pp. 875–877, 2012.

[2] Y. Okawachi, K. Saha, J. S. Levy, Y. H. Wen, M. Lipson, and A. L. Gaeta, "Octave- spanning frequency comb generation in a silicon nitride chip," *Opt. Lett.*, vol. 36, pp. 3398–3400, 2011.

[3] A. G. Griffith et al., "Silicon-chip mid-infrared frequency comb generation," *Nature Commun.*, vol. 6, 2015, Art. no. 6299.

[4] P. Del'Haye, A. Schliesser, O. Arcizet, T. Wilken, R. Holzwarth, and T. J. Kippenberg, "Optical frequency comb generation from a monolithic microresonator," *Nature*, vol. 450, pp. 1214–1217, 2007.

[5] M. G. Suh and K. Vahala, "Gigahertz-repetition-rate soliton microcombs," *Optica*, vol. 5, pp. 65–66, 2018.

[6] T. J. Kippenberg, R. Holzwarth, and S. A. Diddams, "Microresonator based optical frequency combs," *Science*, vol. 332, pp. 555–559, 2011.

[7] I. S. Grudinin, N. Yu, and L. Maleki, "Generation of optical frequency combs with a CaF2 resonator," *Opt. Lett.*, vol. 34, pp. 878–880, 2009.

[8] S. B. Papp and S. A. Diddams, "Spectral and temporal characterization of a fused-quartz microresonator optical frequency comb," *Phys. Rev. A*, vol. 84, 2011, Art. no. 053833.

[9] X. X. Xue et al., "Thermal tuning of kerr frequency combs in silicon nitride microring resonators," *Opt. Exp.*, vol. 24, pp. 687–698, 2016.

[10] T. Kobatake, T. Kato, H. Itobe, Y. Nakagawa, and T. Tanabe, "Thermal Effects on Kerr comb generation in a CaF2 whispering-gallery mode microcavity," *IEEE Photon. J.*, vol. 8, no. 2, Apr. 2016, Art. no. 4501109.

[11] A. A. Savchenkov et al., "Generation of Kerr combs centered at 4.5 μm in crystalline microresonators pumped with quantumcascade lasers," *Opt. Lett.*, vol. 40, pp. 3468–3471, 2015.

[12] C. Y. Wang et al., "Midinfrared optical frequency combs at 2.5 μm based on crystalline microresonators," *Nature Commun.*, vol. 4, 2013, Art. no. 1345.

[13] L. H. Jia et al., "Nonlinear calibration of frequency modulated continuous wave LiDAR based on a microresonator soliton comb," *Opt. Lett.*, vol. 46, pp. 1025–1028, 2021.

[14] S. B. Papp et al., "Microresonator frequency comb optical clock," *Optica*, vol. 1, pp. 10–14, 2014.

[15] W. Liang et al., "High spectral purity Kerr frequency comb radio frequency photonic oscillator," *Nature Commun.*, vol. 6, 2015, Art. no. 7957.

[16] J. Pfeifle et al., "Coherent terabit communications with microresonator Kerr frequency combs," *Nature Photon.*, vol. 8, pp. 375–380, 2014.

[17] Z. C. Zhou et al., "Prospects and applications of on-chip lasers," *eLight*, vol. 3, pp. 1–25, 2023.

[18] P. Trocha et al., "Ultrafast optical ranging using microresonator soliton frequency combs," *Science*, vol. 359, pp. 887–891, 2018.

[19] M. G. Suh, Q. F. Yang, K. Y. Yang, X. Yi, and K. J. Vahala, "Microresonator soliton dual-comb spectroscopy," *Science*, vol. 354, pp. 600–603, 2016.

[20] C. Y. Bao, M. G. Suh, and K. Vahala, "Microresonator soliton dual-comb imaging," *Optica*, vol. 6, pp. 1110–1116, 2019.

[21] E. Vicentini, Z. H. Wang, K. V. Gasse, T. W. Hänsch, and N. Picqué, "Dual-comb hyperspectral digital holography," *Nature Photon.*, vol. 15, pp. 890–894, 2021.

[22] J. K. Jang, A. Klenner, X. C. Ji, Y. Okawachi, M. Lipson, and A. L. Gaeta, "Synchronization of coupled optical microresonators," *Nature Photon.*, vol. 12, pp. 688–693, 2018.

[23] M. J. Yu, Y. Okawachi, A. G. Griffith, N. Picqué, M. Lipson, and A. L. Gaeta, "Silicon-chip-based mid-infrared dual-comb spectroscopy," *Nature Commun.*, vol. 9, pp. 1869, 2018.

[24] N. G. Pavlov et al., "Soliton dual frequency combs in crystalline microresonators," *Opt. Lett.*, vol. 42, pp. 514–517, 2017.

[25] Z. L. Newman et al., "Architecture for the photonic integration of an optical atomic clock," *Optica*, vol. 6, pp. 680–685, 2019.

[26] J. Riemensberger, K. Hartinger, T. Herr, V. Brasch, R. Holzwarth, and T. J. Kippenberg, "Dispersion engineering of thick high-Q silicon nitride ring-resonators via atomic layer deposition," *Opt. Exp.*, vol. 20, pp. 27661–27669, 2012.

[27] H. Zhang et al., "Soliton microcombs multiplexing using intracavity-stimulated Brillouin lasers," *Phys. Rev. Lett.*, vol. 130, 2023, Art. no. 153802.

[28] C. Y. Qin et al., "Co-generation of orthogonal soliton pair in a monolithic fiber resonator with mechanical tunability," *Laser Photon. Rev.*, vol. 7, 2023, Art. no. 2200662.

[29] M. G. Suh and K. J. Vahala, "Soliton microcomb range measurement," *Science*, vol. 359, pp. 884–887, 2018.

[30] S. Fujii et al., "Effect on Kerr comb generation in a clockwise and counter-clockwise mode coupled microcavity," *Opt. Exp.*, vol. 25, pp. 28969–28982, 2017.

[31] Q. F. Yang, X. Yi, K. Y. Yang, and K. Vahala, "Counter-propagating solitons in microresonators," *Nature Photon.*, vol. 11, pp. 560–564, 2017.

[32] Q. F. Yang, X. Yi, K. Y. Yang, and K. Vahala, "Stokes solitons in optical microcavities," *Nature Phys.*, vol. 13, pp. 53–57, 2016.

[33] E. Lucas et al., "Spatial multiplexing of soliton microcombs," *Nature Photon.*, vol. 12, 2018, Art. no. 699.

[34] W. Q. Wang et al., "Dual-pump Kerr micro-cavity optical frequency comb with varying FSR spacing," *Sci. Rep.*, vol. 6, 2016, Art. no. 28501.

[35] J. Y. Zhang, G. L. Hu, K. Y. Zhong, W. Zhou, and H. K. Tsang, "Investigation of low-power comb generation in silicon microresonators from dual pumps," *J. Opt.*, vol. 23, 2021, Art. no. 10LT03.

[36] R. Suzuki, S. Fujii, A. Hori, and T. Tanabe, "Theoretical study on dual-comb generation and soliton trapping in a single microresonator with orthogonally polarized dual pumping," *IEEE Photon. J.*, vol. 11, no. 1, Feb. 2019, Art. no. 6100511.

[37] P. Parra-Rivas, E. Knobloch, D. Gomila, and L. Gelens, "Dark solitons in the Lugiato-Lefever equation with normal dispersion," *Phys. Rev. A*, vol. 93, 2016, Art. no. 063839.

[38] S. Coen, H. G. Randle, T. Sylvestre, and M. Erkintalo, "Modeling of octave-spanning kerr frequency combs using a generalized mean-field Lugiato-Lefever model," *Opt. Lett.*, vol. 38, pp. 37–39, 2013.

[39] Y. K. Chembo and C. R. Menyuk, "Spatiotemporal Lugatio-Lefever formalism for Kerr-comb generation in whispering-gallery-mode resonators," *Phys. Rev. A*, vol. 87, 2013, Art. no. 053852.

[40] L. J. Guo et al., "Mid-infrared dual-comb generation via the cross-phase modulation effect in a normal-dispersion microcavity," *Appl. Opt.*, vol. 59, pp. 2101–2107, 2020.

[41] A. Coillet and Y. Chembo, "On the robustness of phase locking in Kerr optical frequency combs," *Opt. Lett.*, vol. 39, pp. 1529–1532, 2014.

[42] S. Diallo and Y. K. Chembo, "Optimization of primary Kerr optical frequency combs for tunable microwave generation," *Opt. Lett.*, vol. 42, pp. 3522–3525, 2017.

[43] T. Herr et al., "Temporal solitons in optical microresonators," *Nature Photon.*, vol. 8, pp. 145–152, 2014.

[44] J. A. Jaramillo-Villegas, X. X. Xue, P. H. Wang, D. E. Leaird, and A. M. Weiner, "Deterministic single soliton generation and compression in microring resonators avoiding the chaotic region," *Opt. Exp.*, vol. 23, pp. 9618–9626, 2015.

[45] G. P. Agrawal, *Nonlinear Fiber Optics*. New York, NY, USA: Academic, 2013.